Journal of Materials Chemistry A

RSC Publishing

COMMUNICATION

View Article Online
View Journal | View Issue

Thermodynamic-enabled synthesis of Bi/$Bi_{14}Te_6$ axial heterostructure nanowires

Cite this: *J. Mater. Chem. A*, 2013, **1**, 2395

Received 6th September 2012
Accepted 18th December 2012

DOI: 10.1039/c2ta00203e

www.rsc.org/MaterialsA

Joohoon Kang,†‡[a] Wooyoung Shim,†§[b] Seunghyun Lee,[a] Jong Wook Roh,¶[a] Jin-Seo Noh,[a] Peter W. Voorhees*[b] and Wooyoung Lee*[a]

We report thermodynamically controlled multi-segmented nanowires for phonon-glass, electron-crystal materials prepared by on-film formation of nanowires (OFF–ON), which is capable of growing high-quality single-crystalline Bi nanowires by the subsequent sputtering of Te onto the Bi nanowires and by post-annealing. The Bi/$Bi_{14}Te_6$ multi-segmented nanowires exhibit lower thermal conductivities than Bi_xTe_y compounds, while the electrical conductivities of Bi nanowires and multi-segmented nanowires are similar.

Advances in nanowire-based technologies directly rely on the development of nanostructures whose properties are controlled during synthesis. The capability of design and rational synthesis of nanowires as a platform material is therefore a key step towards realizing unprecedented structural and functional building blocks for many applications. Specifically, the capability to create novel nanostructures with tunable composition and structure on many length scales is critical to the unique functional characteristics.[1–4] Thus, designing and synthetically realizing complex nanowire materials allow one to explore the fundamental science and advancing technology.

In this regard, semiconductor nanowires have served as one of the most powerful platforms given that it is possible to synthesize structures in which the composition is modulated along the radial and axial directions of the nanowire, namely, core/shell[5] and superlattice nanowires,[6] respectively. The growth methodology is based on the vapor–liquid–solid (VLS) technique[7] that uses a metallic seed particle forming a low temperature eutectic alloy with the material of the resulting nanowires; this method offers great potential for nanoelectronics,[8] nano-photovoltaics,[9] and biological systems.[10] We have previously developed a nanowire growth method, termed on-film formation of nanowires (OFF–ON),[11] which is a template- and catalyst-free synthetic approach to synthesizing highly crystalline Bi-based nanowires. In the growth process, which is inspired by the problematic issue of whisker formation with a diameter of typically hundreds of micrometers, we utilize thermally induced compressive stress within a polycrystalline thin film to grow nanowires as small as tens of nanometers in diameter. Because of its direct growth capability and compatibility with multi-component materials, OFF–ON can be used to grow single-element (Bi)[11,13–15] and compound nanowires (Bi–Te)[12] in a simple manner.

Furthermore, the composition control in the radial direction was achieved for synthesizing Bi–Te core/shell nanowires that can be used in high-efficiency thermoelectrics. Recently, Zhang *et al.* announced the design principle for Te-based nanostructures. In particular, low thermal conductivity (0.5 W m^{-1} K^{-1}) is obtained by the fabrication of solution assisted Te-based nanowires such as Te–Bi and core/shell nanowires and Te–Bi_2Te_3 heterostructure nanowires, which show promising thermoelectric applications.[16–19] In the context of structure–function relationships,[4] the library of achievable nanowires by OFF–ON is desired to be increased in order to realize a specific targeted application (*i.e.*, Bi–Te-based thermoelectrics), and the axial nanowires are a functionally important material from this perspective. Here, we present a design rule for preparing multi-segmented nanowires composed of Bi/$Bi_{14}Te_6$ segments using OFF–ON. This approach, based on the thermodynamics of the supersaturated phase, presents a potential strategy for adjusting the composition of each segment in order to determine a nanowire's properties, providing a step forward in the synthesis of tailorable nanowire architectures in a predictable fashion. Interestingly, we demonstrate that 100 nm diameter multi-segmented nanowires exhibit a low thermal conductivity (κ) of

[a]*Department of Materials Science and Engineering, Yonsei University, 134 Shinchon, Seoul 120-749, Korea. E-mail: wooyoung@yonsei.ac.kr*

[b]*Department of Materials Science and Engineering, Northwestern University, Evanston, IL 60208, USA. E-mail: p-voorhees@northwestern.edu*

† These authors equally contributed to this work.

‡ Current address: Department of Materials Science and Engineering, Northwestern University, Evanston, IL 60208, USA.

§ Current address: Department of Chemistry and Chemical Biology, Harvard University, Cambridge, MA 02138, USA.

¶ Current address: Advanced Material Research Center, Samsung Advanced Institute of Technology, San 14 Nongseo-dong, Yongin, Korea.

0.92 W m^{-1} K^{-1} and a low electrical resistivity (ρ, high electrical conductivity) of 9.7 × 10^{-4} Ω cm at room temperature, which approaches the amorphous limit for the thermal conductivity and is close to the metallic electrical conductivity of Bi, and thus represents an efficient thermoelectric material.

Unlike previous attempts to prepare Te/Bi_2Te_3 multi-segmented nanowires, where the synthesis begins at the Te-rich phases, our strategy to make Bi/$Bi_{14}Te_6$ multi-segmented nanowires relies on a thermodynamic approach that focuses on the Bi-rich phases (Fig. 1a). This approach allows for Bi/$Bi_{14}Te_6$ formation, rather than Te/Bi_2Te_3 formation, at moderate temperature *via* equilibrium phase transition.[20] Astonishingly, the Bi/$Bi_{14}Te_6$ nanowire architecture has not been investigated in the Bi–Te alloy system so far. According to a binary Bi–Te phase diagram, approximately 30% Te is necessary to form a $Bi_{14}Te_6$ homogeneous nanowire, but in this study, a smaller fraction of Te (<30%) makes the coexistence of both pure Bi and $Bi_{14}Te_6$ phase. In a typical OFF–ON process, a Bi thin film is deposited onto a SiO_2/Si surface by UHV radio frequency (RF) sputtering, and Bi nanowires are grown simply by the subsequent thermal annealing process. This annealing process induces thermal compressive stress within the polycrystalline Bi thin film, which is the driving force for the growth of Bi nanowires with high aspect ratios, uniform diameter, and high-quality crystallinity. Next, a thin Te layer, relative to the volume of Bi, is deposited onto the nanowires by tilting and rotating the sample during low power deposition. Thin Te layers on the relatively high volume Bi nanowires are critical for the synthesis of Bi-based multi-segmented nanowires. In this approach, the total volume of Te with respect to Bi is limited to approximately 20%, and as a result 46% and 34% of the Bi is used to form $Bi_{14}Te_6$ and Bi segments, respectively.

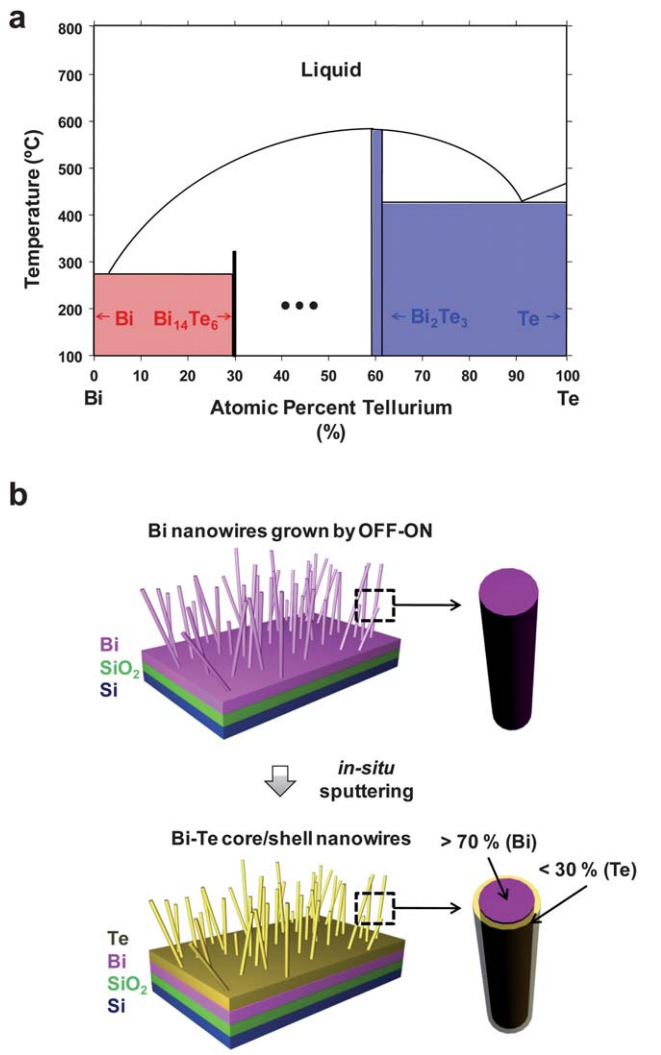

Fig. 1 (a) Bi–Te phase diagram indicates the thermodynamically stable states of Bi_xTe_y compounds. Other intermetallic phases between $Bi_{14}Te_6$ and Bi_2Te_3 are not shown, for clarity. (b) Schematic representations of Bi nanowire fabrication and *in situ* Te deposition. (Step 1) A Bi thin film is deposited onto the SiO_2/Si substrate using UHV RF sputtering. Bi nanowires are grown from the Bi film to release the stored compressive stress during annealing at 260–270 °C for 10 hours. (Step 2) A Te thin film is deposited onto the substrate containing the Bi nanowires using UHV RF sputtering. The Te shell thickness is below 10 nm to fix the atomic ratio between Bi (>70%) and Te (<30%).

Indeed, transmission electron microscope (TEM) images taken in a consecutive time series show the Bi–Te phase transition from two distinct single elements (Bi–Te core/shell) to one composite (Bi/$Bi_{14}Te_6$ multi-segmented) during the annealing process (Fig. 2b–e). As-prepared Bi–Te core/shell nanowires (Fig. 2b) begin to locally form small Bi–Te segregated seeds on the nanowire surface, as shown in Fig. 2c, after annealing at 310 °C for 1 hour. When the nanowire is annealed for 5 hours, BiTe compounds between a pair of Bi regions are formed (Fig. 2d). Interestingly, after the additional 5 hours of annealing, the shape of the Bi regions becomes droplet-like (Fig. 2e).

Fig. 2f schematically illustrates the time-evolution model to account for the formation of Bi/$Bi_{14}Te_6$ multi-segmented nanowires. Immediately after growing single-crystalline Bi nanowires by the OFF–ON method, a thin Te film is deposited onto the Bi nanowires to form Bi–Te core/shell structures using *in situ* RF sputtering with a 30 W deposition power (step 1). The interface between the Bi core and the Te shell becomes atomically rough as a result of elemental inter-diffusion, and it facilitates interfacial thermodynamic reactions. Here, the thickness of the Te shell is below 10 nm where the Te portion in the Bi–Te core/shell nanowire is about 15–20% of the wire diameter. Since the annealing temperature is above the melting point of Bi (see Fig. 1a), upon annealing, the Bi core liquefies. This produces a solid–liquid interface consisting of a solid Te and perhaps Bi alloy (if there is significant solid diffusivity of Bi) and liquid bismuth. The roughness of the solid–vapor interface of Fig. 2c may be due to small $Bi_{14}Te_6$ domains that resulted from diffusion of Bi into the solid Te. The phase diagram shows that Te can dissolve in liquid Bi at this temperature. As the concentration of Te in the liquid increases, $Bi_{14}Te_6$ nucleates. The mobility of the solid–liquid interface along with the nonzero solid–liquid interfacial energy leads to morphological instability of the interface, known as Rayleigh instability, which accompanies the formation of $Bi_{14}Te_6$. As the instability develops, the solid–liquid interfaces from opposite sides of the wire eventually touch and the liquid pinches off, leaving regions

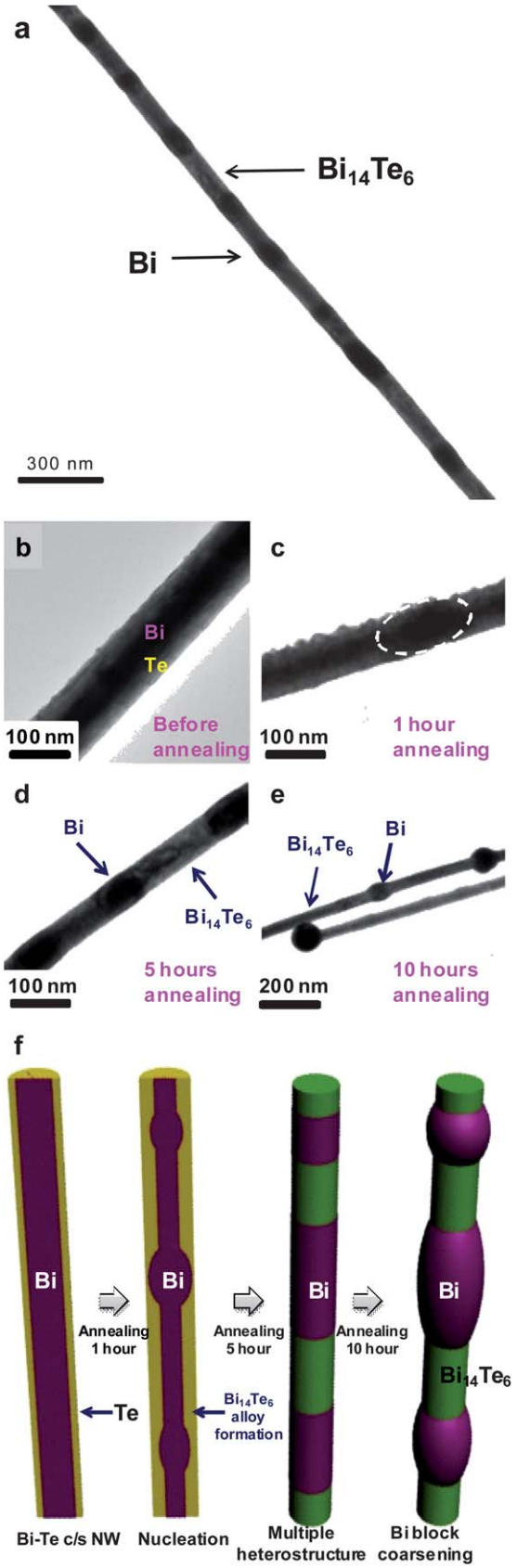

Fig. 2 (a) Zoomed-out TEM image of an individual Bi–$Bi_{14}Te_6$ multi-segmented nanowire. (b) Low magnification TEM image of an individual Bi–Te core/shell nanowire (before annealing). (c) Bi-segregated region (white dashed-line) is locally formed in the nanowire after annealing at 310 °C for 1 hour. (d) After annealing for 5 hours, Bi and $Bi_{14}Te_6$ blocks are separated. (e) After the additional 5 hours of annealing, the shape of Bi regions becomes droplet-like. (f) Schematic of the time-evolution model to synthesize Bi/$Bi_{14}Te_6$ multi-segmented nanowires. (Step 1) Bi nanowires are fabricated by the OFF–ON method. And the Te thin film is deposited below 10 nm. (Step 2) After 1 hour annealing, the Bi region is nucleated. (Step 3) Bi segments are separated from BiTe compounds *via* Rayleigh instability. (Step 4) Bi regions are coarsened to droplet-like shape to reduce surface energy with a concomitant change in the length of the $Bi_{14}Te_6$ regions. Each step 1 to 4 is matched to (b) to (e).

of liquid, which are nearly pure liquid Bi, and solid $Bi_{14}Te_6$ (see Fig. 2d). The Rayleigh instability of a tube occurs on length scales that are approximately equal to the diameter of the wire. Thus the distance between the Bi domains should be approximately 3 times the diameter of the wire, which is the case. Upon further annealing, the liquid Bi regions change their morphology to more drop-like shapes separated by larger regions of $Bi_{14}Te_6$. This is essentially a classical coarsening process where the system reduces the total liquid Bi–vapor interfacial area, along with a change of the contact angle at the liquid–vapor–solid tri-junction. Thus with increasing annealing time, the contact angles increase, the droplets appear rounder and the length of the $Bi_{14}Te_6$ regions increases. This change occurs by the diffusion of Bi either through the $Bi_{14}Te_6$ or along its surface, allowing the liquid Bi regions to communicate diffusionally. Thus, our method demonstrates that single-crystalline Bi/$Bi_{14}Te_6$ multi-segmented nanowires can be fabricated by a combination of simple processes, *i.e.*, OFF–ON, *in situ* sputtering, and post-annealing.

Following the synthesis of the multi-segmented nanowires, high-resolution TEM analysis reveals that this synthetic protocol yields high-quality, single-crystal multi-segmented nanowires with sharp interfaces (Fig. 3). TEM images of a Bi/$Bi_{14}Te_6$ nanowire grown after 10 hour post-annealing show that both the Bi and $Bi_{14}Te_6$ segments are highly ordered, and selected area electron diffraction (SAED) patterns (insets of Fig. 3a and b) further confirm the single-crystal nature of each segment and assign the growth directions as [110] and [$3\bar{3}3$]. Fig. 3c shows the atomically abrupt boundary between the Bi and $Bi_{14}Te_6$ segments. Interplanar spacings are measured to be 4.53 Å and 4.47 Å for the Bi and $Bi_{14}Te_6$ segments, respectively. Fig. 3d shows a high angle annular dark field (HAADF) image of unit segments of a Bi/$Bi_{14}Te_6$ multi-segmented nanowire. Here, the brighter region (convex part) is the Bi segment, while the darker region (straight part) is the $Bi_{14}Te_6$ segment. Energy dispersive X-ray spectroscopy (EDX) was used to analyze elemental distribution in our Bi/$Bi_{14}Te_6$ multi-block nanowires. From the element mapping images of the respective segments, we confirm that the brighter region is filled only with Bi (Fig. 3e), whereas the darker region consists of 70% Bi and 30% Te (Fig. 3f), which corresponds to the atomic ratio of 14 : 6. The measured atomic composition of 70% of Bi and 30% of Te represents a stoichiometric compound, $Bi_{14}Te_6$, which is an equilibrium phase for Bi–Te as determined from its phase diagram. Finally, we evaluate the potential applicability of our multi-segmented nanowires as a thermoelectric material. First, to evaluate the electrical conductivity, four-point probe

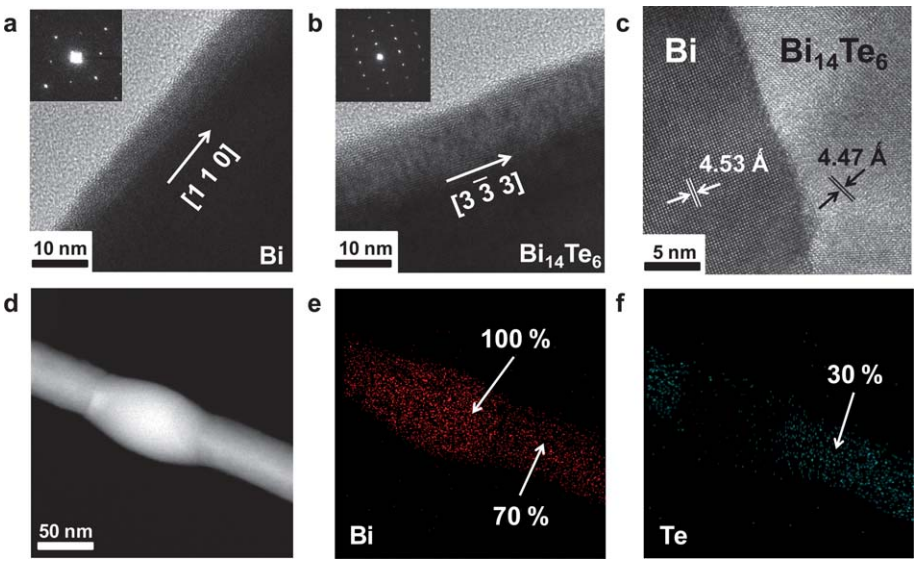

Fig. 3 (a) and (b) High resolution TEM images of Bi and $Bi_{14}Te_6$ segments show high-quality single crystalline multi-segmented nanowires (insets indicate single-crystal and the growth directions as [110] and [3$\bar{3}$3], respectively). (c) The atomically abrupt boundary between Bi and $Bi_{14}Te_6$ segments. (d) HAADF image of unit segments of a Bi/$Bi_{14}Te_6$ multi-segmented nanowire. The brighter region is the Bi segment and the darker region is the $Bi_{14}Te_6$ segment. (e) and (f) The element mapping images represent 100% Bi in the convex region and 70% Bi (red) and 30% Te (cyan) in the straight region which corresponds to the atomic ratio of 14 : 6.

conductivity measurements of the multi-segmented nanowires were conducted (Fig. 4a) for the 104 nm and 308 nm diameter multi-segmented nanowires. The measured electrical resistivity was 9.7×10^{-4} Ω cm for 104 nm and 8.8×10^{-4} Ω cm for 308 nm Bi/$Bi_{14}Te_6$ multi-segmented nanowires (Fig. 4b). These values are comparable to those of pure Bi nanowires with similar diameters, namely 7.7×10^{-4} Ω cm for 98 nm and 5.6×10^{-4} Ω cm for 284 nm Bi nanowires. The resistivity of $Bi_{14}Te_6$

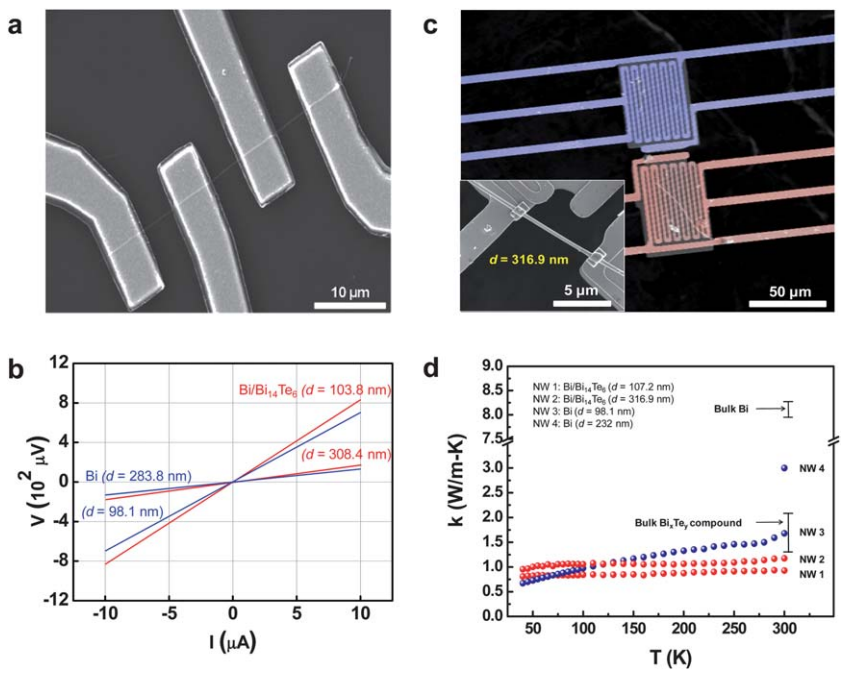

Fig. 4 (a) Four-point probe device is utilized to measure the electrical conductivity of the multi-segmented nanowires. (b) The measured electrical resistivity is 9.7×10^{-4} Ω cm for 104 nm and 8.8×10^{-4} Ω cm for 308 nm Bi/$Bi_{14}Te_6$ multi-segmented nanowires (red lines) and 7.7×10^{-4} Ω cm for 98 nm and 5.6×10^{-4} Ω cm for 284 nm Bi nanowires (blue lines). (c) SEM image of a suspended MEMS device to measure the thermal conductivity of an individual Bi/$Bi_{14}Te_6$ multi-segmented nanowire. The inset indicates local Pt/C composite deposition using a dual-beam FIB to minimize thermal contact resistance between the nanowire and the membrane. (d) The measured temperature dependence of thermal conductivity in Bi/$Bi_{14}Te_6$ multi-segmented nanowires (d = 107 nm and 317 nm, red lines) and Bi nanowires (d = 98 nm and 232 nm,[26] blue line). The thermal conductivity range of bulk Bi and Bi_xTe_y compounds at room temperature is also indicated.

nanowires can be estimated using Ohm's law for 104 nm and 308 nm segments. Since the electric field and current are perpendicular to the segments, the current density of Bi is the same as that of $Bi_{14}Te_6$, $J_{total} = J_{Bi} = J_{Bi_{14}Te_6}$. Therefore, the electric field is expressed as $E_{total} = f_{Bi}E_{Bi} + f_{Bi_{14}Te_6}E_{Bi_{14}Te_6} = (f_{Bi}\rho_{Bi} + f_{Bi_{14}Te_6}\rho_{Bi_{14}Te_6})J_{total}$, where f_{Bi} ($\sim$1/3) and $f_{Bi_{14}Te_6}$ ($\sim$2/3) are the volume fractions of Bi and $Bi_{14}Te_6$ segments. From the relation $\rho_{Bi/Bi_{14}Te_6} = f_{Bi}\rho_{Bi} + f_{Bi_{14}Te_6}\rho_{Bi_{14}Te_6}$, the resistivity of 104 nm and 308 nm $Bi_{14}Te_6$ segments is estimated as 1.1×10^{-3} Ω cm and 1.0×10^{-3} Ω cm, respectively. The electrical conductivities of bulk Bi and $Bi_{14}Te_6$ are known to be 1×10^{-4} Ω cm and 6.0×10^{-4} Ω cm, respectively.[21–23] An increased resistivity in all nanowires, compared to their bulk counterparts, may arise from the surface scattering of charge carriers.[24–26] Nevertheless, the electrical resistivity of $Bi/Bi_{14}Te_6$ multi-segmented nanowires, compared to pure Bi nanowires, was relatively preserved, and as a consequence, the electrical conductivity.

Second, to evaluate the suppression of lattice thermal conductivity, κ_L, the thermal conductivity of individual multi-segmented nanowires was measured using the suspended MEMS devices.[25,26] Each MEMS device has two suspended silicon nitride (SiN_x) membranes, a heating membrane and a sensing membrane, and each membrane is suspended by five metal line patterned SiN_x legs that play a role in making electric connection (Fig. 4c). Fig. 4d shows the temperature dependence of κ in individual $Bi/Bi_{14}Te_6$ nanowires (d = 107 nm and 317 nm) whose diameters are similar to those of the multi-segmented nanowires used in previous electrical conductivity measurements (d = 104 nm and 308 nm). The κ of the nanowires is 0.92 W m^{-1} K^{-1} for the 107 nm diameter nanowire and 1.18 W m^{-1} K^{-1} for the 317 nm diameter nanowire at room temperature. For comparison, the κ of a pure Bi nanowire with a similar diameter (d = 98 nm) was measured, and the κ range of homogeneous Bi_xTe_y compounds at room temperature is indicated in Fig. 4d. We calculated the suppression of the lattice thermal conductivity, κ_L, in the 107 nm diameter multi-segmented nanowire. κ_L for the 107 nm multi-segmented nanowire was obtained by subtracting κ_E, which can be calculated using the Wiedemann–Franz law, $\kappa_E = L\sigma T$, where L is the Lorenz number, σ is the electrical conductivity and T is the absolute temperature. The Lorenz number for a 1-D metal nanowire is smaller than that for its bulk counterpart,[27–30] and thus the lower limit of the Lorenz number,[31] 2.2×10^{-8} W Ω K^{-2}, is used for the calculations for the 107 nm multi-segmented nanowire. With measured κ_{total} and σ for the 107 nm multi-segmented nanowire at room temperature, κ_E and κ_L are 0.69 and 0.23 W m^{-1} K^{-1}, respectively. For comparison, κ_E and κ_L for the 98 nm pure Bi nanowire are also calculated and are 0.87 and 0.74 W m^{-1} K^{-1}, respectively. It is worth noting that κ_L is suppressed more than κ_E in the multi-segmented nanowires, but the exact mechanism to explain this κ_L suppression in $Bi/Bi_{14}Te_6$ multi-segmented nanowires is not clear.

In conclusion, we have presented a method to prepare $Bi/Bi_{14}Te_6$ multi-segmented nanowires using a thermodynamic approach in the supersaturated Bi–Te core/shell nanowires. The advantages of this method include its simplicity and the avoidance of cross-contamination or damage in the resultant nanowires as catalysts and templates are not used. Importantly, our multi-segmented nanowires show low thermal conductivity but uncompromised electrical conductivity which is critical for realizing high-efficiency thermoelectric applications. This study has focused on the electrical and thermal conductivity, which together with the Seebeck coefficient will determine ZT. The Seebeck coefficient, which is more relevant to density of states engineering, warrants further study. At present, the length of each segment is limited by the thermodynamic equilibrium composition. For example, a higher Bi composition in our design will likely lead to a longer Bi segment. We expect that as the understanding of the relationships between the atomic compositions, temperature, annealing time, and the resultant segment length matures, the number and type of multi-segmented nanowires accessible through this approach for many applications should significantly increase.

Acknowledgements

This work was supported by the Agency for Defense Development (ADD), under agreement number ADD-10-70-07-03, the Pioneer Research Center Program (2010-0019313), and the Priority Research Centers Program (2009-0093823) through the National Research Foundation of Korea (NRF).

References

1 C. M. Lieber, *MRS Bull.*, 2011, **36**, 1052–1063.
2 B. Tian and C. M. Lieber, *Pure Appl. Chem.*, 2011, **83**, 2153–2169.
3 W. Lu and C. M. Lieber, *Nat. Mater.*, 2007, **6**, 841.
4 C. M. Lieber and Z. L. Wang, *MRS Bull.*, 2007, **32**, 99.
5 L. J. Lauhon, M. S. Gudiksen, D. Wang and C. M. Lieber, *Nature*, 2002, **420**, 57.
6 M. S. Gudiksen, L. J. Lauhon, J. Wang, D. Smith and C. M. Lieber, *Nature*, 2002, **415**, 617.
7 A. M. Morales and C. M. Lieber, *Science*, 1998, **279**, 208.
8 H. Yan, H. S. Choe, S. Nam, Y. Hu, S. Das, J. F. Klemic, J. C. Ellenbogen and C. M. Lieber, *Nature*, 2011, **470**, 240–244.
9 B. Tian, X. Zheng, T. J. Kempa, Y. Fang, N. Yu, G. Yu, J. Huang and C. M. Lieber, *Nature*, 2007, **449**, 885–889.
10 B. Tian, T. Cohen-Karni, Q. Qing, X. Duan, P. Xie and C. M. Lieber, *Science*, 2010, **329**, 830–834.
11 W. Shim, J. Ham, K. I. Lee, W. Y. Jeung, M. Johnson and W. Lee, *Nano Lett.*, 2009, **9**, 18.
12 J. Ham, W. Shim, D. H. Kim, S. Lee, J. W. Roh, S. W. Sohn, K. H. Oh, P. W. Voorhees and W. Lee, *Nano Lett.*, 2009, **9**, 2867.
13 W. Shim, D. H. Kim, K. I. Lee, K. J. Jeon, J. Ham, J. Y. Chang, S. H. Han, W. Y. Jeung, M. Johnson and W. Lee, *J. Appl. Phys.*, 2008, **105**, 073715.
14 W. Shim, J. Ham, J. Kim and W. Lee, *Appl. Phys. Lett.*, 2009, **95**, 232107.
15 J. Ham, W. Shim, D. H. Kim, K. H. Oh, P. W. Voorhees and W. Lee, *Appl. Phys. Lett.*, 2011, **98**, 043102.

16 J. Kang, J. W. Roh, W. Shim, J. Ham, J.-S. Noh and W. Lee, *Adv. Mater.*, 2011, **23**, 3414.
17 G. Zhang, Q. Yu, W. Wang and X. Li, *Adv. Mater.*, 2010, **22**, 1959.
18 G. Zhang, W. Wang and X. Li, *Adv. Mater.*, 2008, **20**, 3654.
19 G. Zhang, H. Fang, H. Yang, L. Jauregul, Y. Chen and Y. Wu, *Nano Lett.*, 2012, **12**, 3627.
20 T. B. Massalski, *Binary Alloy Phase Diagrams*, Am. Soc. Metals, 1986.
21 G. K. White and S. B. Woods, *Philos. Mag.*, 1958, **3**, 342.
22 J. W. Roh, K. Hippalgaonkar, J. Ham, R. Chen, M. Z. Li, P. Ercius, A. Majumdar, W. Kim and W. Lee, *ACS Nano*, 2011, **5**, 3954.
23 J. W. G. Bos, H. W. Zandberge, M.-H. Lee, N. P. Ong and R. J. Cava, *Phys. Rev. B: Condens. Matter Mater. Phys.*, 2007, **75**, 195203.
24 J. W. Roh, S. Y. Jang, J. Kang, S. Lee, J.-S. Noh, W. Kim, J. Park and W. Lee, *Appl. Phys. Lett.*, 2010, **96**, 103101.
25 D. Li, Y. Wu, P. Kim, L. Shi, P. Yang and A. Majumdar, *Appl. Phys. Lett.*, 2003, **83**, 2934.
26 L. Shi, D. Li, C. Yu, W. Y. Jang, D. Kim, Z. Yao, P. Kim and A. Majumdar, *J. Heat Transfer*, 2003, **125**, 881.
27 A. L. Moore, M. T. Pettes, F. Zhou and L. Shi, *J. Appl. Phys.*, 2009, **106**, 034310.
28 Z. M. Zhang, *Microscale Heat Transfer*, McGraw-Hill, 2006, ch. 5.
29 M. N. Tripathi, C. M. Bhandari and M. P. Singh, *Phys. B*, 2010, **405**, 4818.
30 A. J. Minnich, M. S. Dresselhaus, Z. F. Ren and G. Chen, *Energy Environ. Sci.*, 2009, **2**, 466.
31 A. I. Hochbaum, R. Chen, R. D. Delgado, W. Liang, E. C. Garnett, M. Najarian, A. Majumdar and P. Yang, *Nature*, 2007, **451**, 163.

